Key Points:
- Interlinked flux tubes and FTEs were observed in a three-dimensional MHD simulation
- The interlinked flux tubes exhibit the same typical signatures of a flux rope; topology analysis shows that it is not a flux rope
- The interlinked flux tubes are generated due to accumulation of IMF and the formation of multiple magnetic reconnection lines

Correspondence to:
G. Farinas Perez,
german.farinas@gmail.com

Generation Mechanism for Interlinked Flux Tubes on the Magnetopause

G. Farinas Perez[1,2,3], **F. R. Cardoso[2,4]**, **D. Sibeck[1]**, **W. D. Gonzalez[2]**, **G. Facskó[1,3,5]**, **J. C. Coxon[6]**, and **A. D. Pembroke[1,3]**

[1] NASA Goddard Space Flight Center, Greenbelt, MD, USA, [2] INPE Instituto Nacional de Pesquisas Espaciais, São José dos Campos, São Paulo, Brazil, [3] Catholic University of America, Washington, DC, USA, [4] EEL/USP Escola de Engenharia de Lorena/Universidade de São Paulo, Lorena, Brazil, [5] Research Center for Astronomy and Earth Sciences, Geodetic and Geophysical Institute, Hungarian Academy of Sciences, Sopron, Hungary, [6] School of Physics and Astronomy, University of Southampton, Southampton, UK

Abstract We use a global magnetohydrodynamics simulation to analyze transient magnetic reconnection processes at the magnetopause. The solar wind conditions have been kept constant, and an interplanetary magnetic field with large duskward B_Y and southward B_Z components has been imposed. Five flux transfer events (FTEs) with clear bipolar magnetic field signatures have been observed. We observed a peculiar structure defined as interlinked flux tubes (IFTs) in the first and fourth FTE, which had very different generation mechanisms. The first FTE originates as an IFTs and remains with this configuration until its final moment. However, the fourth FTE develops as a classical flux rope but changes its 3-D magnetic configuration to that of IFTs. This work studies the mechanism for generating IFTs. The growth of the resistive tearing instability has been identified as the cause for the first IFTs formation. We believe that the instability has been triggered by the accumulation of interplanetary magnetic field at the subsolar point where the grid resolution is very high. The evidence shows that two new reconnection lines form northward and southward of the subsolar region. The IFTs have been generated with all the classical signatures of a single flux rope. The other IFTs detected in the fourth FTE developed as a result of magnetic reconnection inside its complex and twisted magnetic fields, which leads to a change in the magnetic configuration from a flux rope of twisted magnetic field lines to IFTs.

1. Introduction

Magnetic reconnection is the process whereby magnetic energy is converted into kinetic and thermal energy in physical plasmas. It produces changes of global magnetic topology due to magnetic connectivity. After magnetic field lines reconnect, the newly merged lines exhibit a mixture of plasma from both sides of the current sheet. The merged field lines are expelled from the reconnection region due to magnetic curvature forces. The outgoing plasma is accelerated, and magnetic energy is converted into kinetic energy.

Instabilities in the current sheet, such as the tearing instability, produce reconnection in an inherently time-dependent way with impulsive and bursty releases of energy. Magnetic structures, named flux transfer events (FTEs), form during this transient magnetic reconnection process. Although some characteristics of FTEs were first reported by Haerendel et al. (1978), the description and terminology that we currently use was given by Russell and Elphic (1978) who observed two important characteristic of FTEs. First, during their passage by a satellite, the normal magnetic field to the magnetopause (B_N) exhibits a change of polarity that is caused by the draping of magnetospheric and magnetosheath field lines around the flux tube. The second important characteristic is the enhancement of the core magnetic field (B_M) at the center of the structure due to the tension on the flux tube field lines, which is larger as compared with the surrounding magnetospheric and magnetosheath field lines (Paschmann et al., 1982).

Lee and Fu (1985) showed that when magnetic reconnection occurs in multiple X-reconnection lines, instead of the single line as proposed by Dungey (1961), then FTEs are naturally formed. In the multiple X-line reconnection model the central line is the reconnection line that corresponds to the Gonzalez and Mozer (1974) model and it extends around the dayside magnetopause. The others reconnection lines have a limited extent

and are located southward and northward the extended reconnection line. If reconnection takes place at multiple X-lines this leads to the formation of two helical flux tubes, one in each hemisphere.

Multiple X-lines can be created due to the development of the tearing instability at the subsolar magnetopause. Lee and Fu (1985) used two-dimensional magnetohydrodynamic (MHD) simulations to show that when the characteristic length of the system is much greater than the current layer separating the two plasma regions, the current sheet becomes unsteady and the tearing instability grows at substantial rates, generating large islands. This is a typical scenario at the dayside magnetopause, where the thickness of the current layer is $\simeq$500 km. The new reconnection lines appear at the X points between the magnetic islands. In the presence of a finite B_Y magnetic islands become flux tubes embedded in the magnetopause with a helical field inside. As these tubes grow in size, reconnection slows down and stops. Reconnection will begin again when the saturated magnetic flux tubes convect out of the reconnection region. The presence of B_Y is essential for the formation of flux tube with helical fields. If $B_Y = 0$, this model leads to the formation of isolated magnetic loops instead of helical flux tubes.

Cardoso et al. (2013) studied the formation of FTEs and magnetic reconnection at the subsolar magnetopause using a global 3-D MHD simulation for a large amplitude southward and duskward interplanetary magnetic field (IMF). Cardoso et al. (2013) main finding was the detection of an FTE formed by two interlinked flux tubes (IFTs) which they suggested originated due to magnetic reconnection at different places away from the subsolar point. Single virtual satellite observation and magnetic topology analysis were used to detect this structure. However, they did not provide a clear explanation of how this structure was generated and evolved. To that extent it is necessary to incorporate further analysis in addition to magnetic topology.

The goal of this paper is to study in more detail how the IFTs were generated. For that purpose, we reexamine the output files from the Cardoso et al. (2013) simulation run. The new work and results of this paper will be described as follow. We determine all FTE occurrences in the entire simulation. We measure the onset time, lifetime, magnetic field signatures, speed, and direction of propagation of all five FTEs detected, and we named them FTE1, FTE2, FTE3, FTE4, and FTE5 where FTE1 was the first detected and FTE5 the last. We identify FTE1 as two IFTs, which confirms the interpretation of Cardoso et al. (2013). We calculate the magnetopause as an isosurface of $B_Z = 0$ and compute the topology over this surface; with this technique we show how the IMF accumulates at the subsolar point and develops the instability that we believe originates the IFTs observed in FTE1. In addition to the magnetic topology analysis, the evolution of the IFTs is studied also in terms of the magnetic and plasma properties. A plasmoid with rotational magnetic field and plasma flow vortices has been detected in this structure. We measure more precisely the extent and location of the newly magnetic reconnection lines created by the instability; these lines play an important role in the formation and development of the IFTs. We also observed the occurrence of IFTs in FTE4. We proposed a generation mechanism for both IFTs observed in our simulation. The generation mechanism of the IFTs detected in FTE1 and in FTE4 is compared.

In this paper, we describe the methodology in section 2. The observation and properties of the FTEs are discussed in section 3. The structure, topology, and generation mechanism of the IFTs in FTE1 are analyzed in section 3.1. We provide more details about the creation of multiple X-lines due to the resistive tearing instability in section 3.2. The generation of IFTs in FTE4 due to changes in its 3-D structure is discussed in section 3.3. We show our conclusions in section 4.

2. Methodology

We use a computational simulation to study the FTEs. The code used is the Block-Adaptive-Tree-Solarwind-Roe-Upwind-Scheme (BATS-R-US) and was developed by the Center for Space Environment Modeling at the University of Michigan. The BATS-R-US code solves the three-dimentional ideal MHD equations in volume finite form using numerical methods related to the Riemman solver (Powell et al., 1999; Tóth et al., 2012). The 3-D global MHD simulations we used for our study were performed at the Community Coordinated Modeling Center (CCMC).

The initial solar wind conditions of the run have been set at 5 n/cc for solar wind density and 600 km/s for the solar wind velocity X component. The IMF components have been set to $B_X = 0$ nT, $B_Y = 15.81$ nT, and $B_Z = -15.81$ nT, which corresponds with a clock angle of 135°. Analyzing the simulation files in more detail,
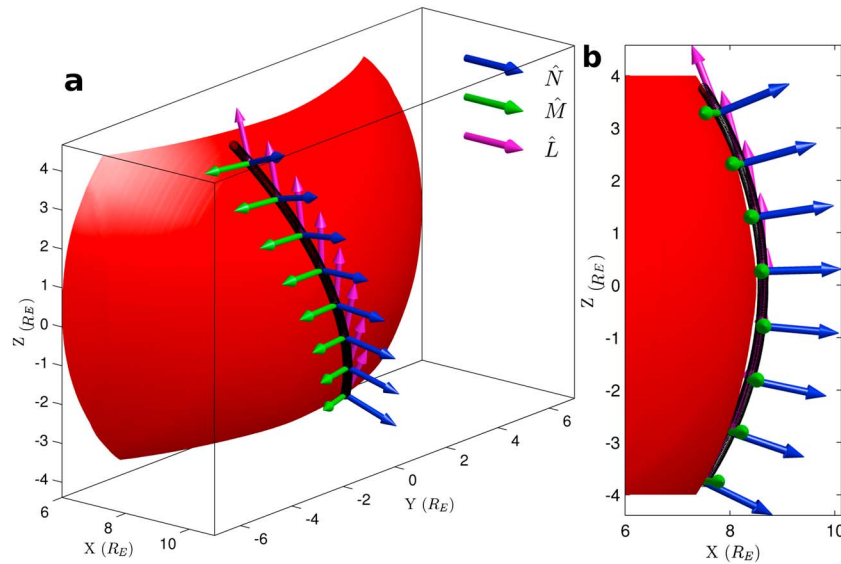
Figure 1. Illustration of the path chosen to plot the magnetic and plasma data using the Shue et al. (1997) model. The vector basis of this system is represented as follows: $\hat{N}$, blue arrow pointing normal to the magnetopause; $\hat{M}$, green arrow; and $\hat{L}$ color magenta arrow. The red surface represents an isosurface of $B_Z = 0$. (a) Three-dimensional view, the Sun is to the right and the Earth to the left. (b) Same as (a) but the view is from the negative y axis. In this perspective it is shown that the path is very close to the magnetopause.

we find out that the correct values of the IMF components are the ones reported here (and not $B_Y = 14$ nT and $B_Z = -14$ nT as reported by Cardoso et al., 2013). The dipole tilt angle is 0°. The coordinate system used is geocentric solar magnetospheric (GSM). The total time of the run is 45 min. The time format we use is minutes: seconds, for example, time 15:30 refers to min 15 and 30 s after the start of the simulation. The time resolution is 15 s, that is, we get an output every 15 s.

We look for signatures of unsteady magnetic reconnection in the magnetopause, specifically FTEs. The magnetopause boundary layer has an approximately thickness of 500 km (Berchem & Russell, 1982), and we used a grid resolution of $\frac{R_E}{32} \sim 200$ km. High resolution in the magnetopause is required to detect the disturbances near the magnetopause current layer that cause FTE signatures.

In global MHD models, magnetic reconnection occurs due to the numerical dissipation (numerical resistivity). Raeder (2006) demonstrated that successful simulations of FTEs depend on the numerical resolution of the model. For a resolution of 0.08 R_E, the numerical dissipation is suppressed sufficiently for FTEs form and survive. We use a finer resolution of $\frac{R_E}{32} \approx 0.03\ R_E$ at the magnetopause. Therefore, the numerical resistivity in our simulation is significantly smaller than that of Raeder (2006), as numerical resistivity is related to the grid resolution.

We detect the FTEs using single and multiple virtual satellites. The single satellites were placed at fixed positions in the Northern or Southern Hemispheres near the subsolar region (Figure 3), and they measure the temporal variation of the magnetic field. The multiple satellites were also fixed in positions along a curve parallel to the subsolar magnetopause (black line in Figure 1), and they monitor the temporal and spatial variation of the magnetic field along this line.

The curve was generated in the following manner. First, the subsolar magnetopause is calculated as an isosurface of $B_Z = 0$, which is represented in Figure 1 (red surface). The distance to the subsolar magnetopause is 8.44 R_E at about 20:00. A distance slightly greater than this is substituted in the following formula of the (Shue et al., 1997) model for the magnetopause in the meridional plane:

$$r = r_0 \left(\frac{2}{1 + \cos\theta} \right)^\alpha \tag{1}$$

where r is the radial distance and θ is the solar zenith angle. This model has two parameters, r_0 and α, representing the standoff distance of the subsolar magnetopause and the level of tail aperture, respectively. We used a standoff distance of $r_0 = 8.62\ R_E$ and a value of $\alpha = 0.05$. Using these values we calculated a curve
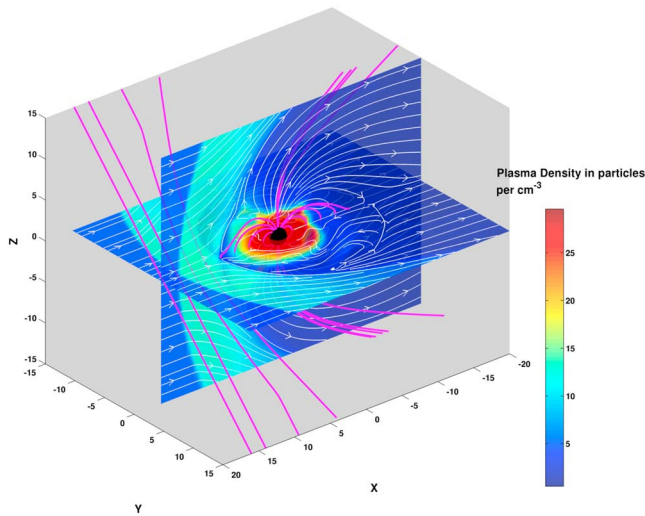
Figure 2. Global perspective of the interaction of the solar wind with the Earth's magnetosphere simulated by the Block-Adaptive-Tree-Solarwind-Roe-Upwind-Scheme code. The pink lines represent the IMF and dipolar magnetic field. The white solid lines with arrows represent velocity streamlines. Two cuts are shown, one at $Y = 0$ and the other at $Z = 0$. The color code indicates the plasma density. The Sun is on the left, and the Earth is represented as a black sphere in the center.

that fit very well with the magnetopause. Due to the IMF has a finite Y component, the FTEs do not move northward or southward but rather northward and downward or southward and duskward. So we rotate the quasi-parabolic curve by trial and error until we find an orientation that captures the largest bipolar signature. This rotation was 30° counterclockwise taking as reference the Z GSM axis. We believe that the orientation that captures the largest bipolar signature is a good approximation of the direction of the FTEs propagation.

For every specific time of the run we measure the magnetic and plasma data at 300 samples along the line path. The normal vector to the magnetopause $\hat{N}$ is calculated deriving the normal in spherical coordinates for the curve in Figure 1 (equation (1)). The vectors $\hat{M}$ and $\hat{L}$ are calculated, respectively, as $\hat{M} = \hat{N} \times \hat{z}_{GSM}$ and $\hat{L} = \hat{M} \times \hat{N}$. Finally, we transform the B_X, B_Y, B_Z components into B_N, B_M, B_L using as basis the $\hat{L}, \hat{M}, \hat{N}$ vectors. Figure 1a shows for a few points the normal boundary system basis vectors. Figure 1b shows the curve and the normal boundary system for a view from the negative y axis.

This method is essentially a spatial plot through a trajectory very close to the magnetopause, starting from the point $X = 7.5R_E$, $Y = 2.17R_E$, $Z = -3.75R_E$ and ending at $X = 7.5R_E$, $Y = -2.17R_E$, $Z = 3.75R_E$, that is, from southern dusk quadrant to northern-dawn quadrant.

3. Results

A global view of the interaction of the solar wind with the Earth's magnetosphere in our MHD simulation can be seen in Figure 2. The orientation of the IMF (pink lines) and the formation of the magnetosheath (green region of density $\approx$10 particles per cm^{-3}) can be observed. The plasma flow is represented by the white solid lines with arrows.

From a global point of view of our simulation, the subsolar bow shock lies around 14 R_E from Earth, the subsolar magnetopause is about 8.5 R_E and the thickness of the magnetosheath is approximately 5.5 R_E. The plasma density in the magnetosheath is about 10 cm^{-3} which is low compared to typical conditions. The low density and the higher thickness of the magnetosheath are due to the strong IMF. For intense IMF the solar wind Alfvén speed increases, so the Alfvén Mach number is lower than for the small IMF case. A low Mach number means that the bow shock is not close to the compression limit of 4; therefore, the magnetosheath is less compressed for large IMF (Lopez et al., 2010).

The solar wind and IMF parameters were kept constant during the whole simulation run, confirming that FTEs can develop spontaneously without changes of the solar wind conditions (Cardoso et al., 2013; Raeder, 2006) .

Figure 3 shows the magnetic field at two specific points near the subsolar magnetopause. The probes were placed in the Northern Hemisphere at $x = 8.5R_E$, $y = -0.3$ R_E, $z = 0.7R_E$ (Figure 3a) and in the Southern Hemisphere at $x = 8.5R_E$, $y = 0.8R_E$, $z = -1R_E$ (Figure 3b). The first probe was located in the northern dawn quadrant ($Z > 0$, $Y < 0$) and the second in the southern dusk quadrant ($Z < 0$, $Y > 0$). The two points were chosen because the magnetic signatures of the FTEs were observed most clearly at these particular locations. This is consistent with the fact that the flow direction is normal to the single magnetic reconnection line tilted from southern dawn to northern dusk at the beginning of the simulation (Cardoso et al., 2013).

The typical bipolar B_N FTE signature can be observed in the first plot of Figure 3a. Three events have been detected by the probe in the Northern Hemisphere. The first takes place at about 29:00 (minutes:seconds) into simulation (FTE1), the second at about 32:00 (FTE2), and the third at about 40:00 (FTE4). In all the cases the normal magnetic field B_N first turns outward to the magnetopause ($+$ positive) followed by an inward ($-$ negative) perturbation of B_N. Therefore, the polarity of the bipolar signature is of the "direct" ($+/-$) kind (Cowley, 1982).

Figure 3b shows the magnetic field data at a point located near the subsolar point but southward of the equator (South Hemisphere). Two bipolar signatures of the B_N component were detected by the probe
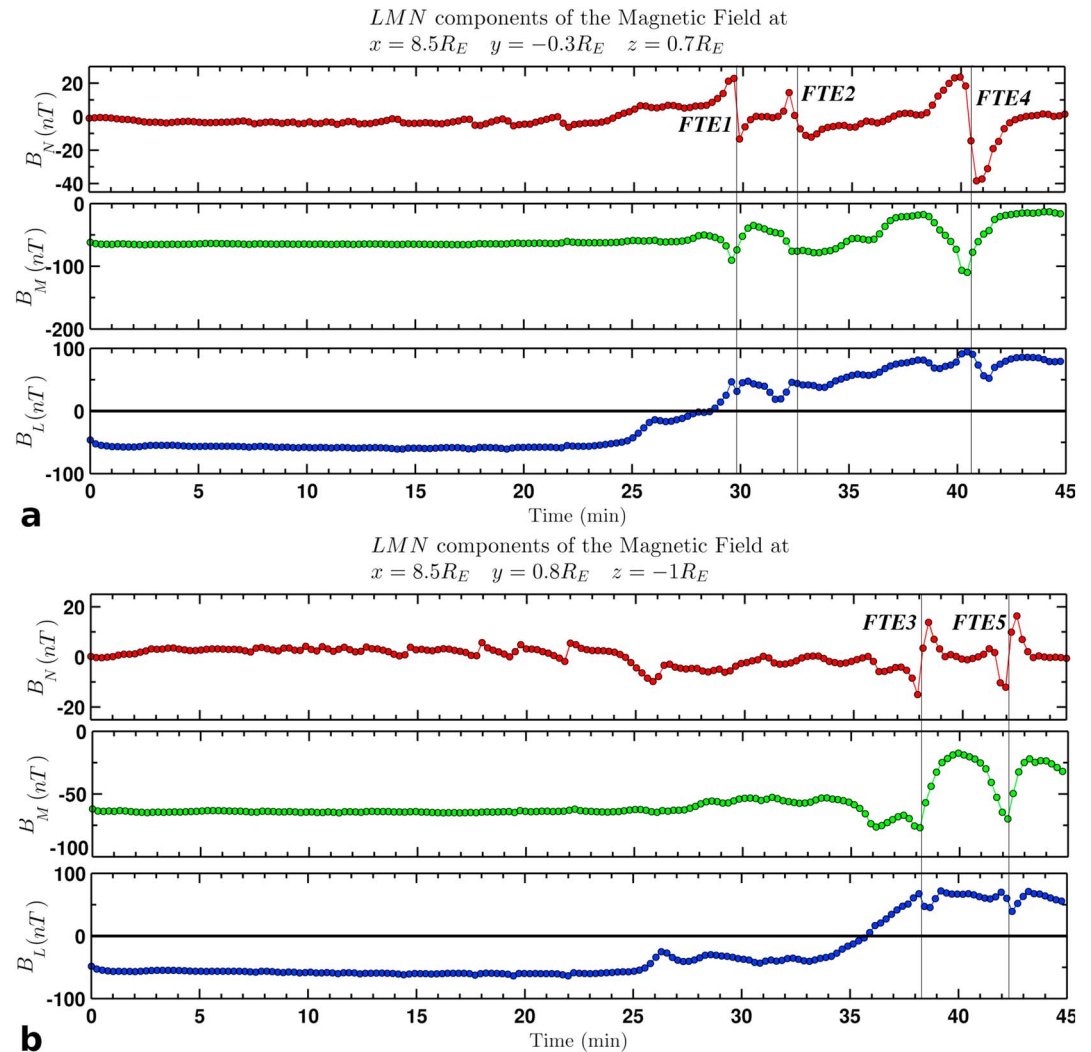
Figure 3. Observations of the simulated magnetic field in boundary normal coordinate system close to the magnetopause. The circle indicate samples taken every 15 s by the virtual probe. (a) The probe is located in the Northern Hemisphere at $x = 8.5\ R_E$, $y = -0.3\ R_E$, and $z = 0.7\ R_E$. (b) The probe is located in the Southern Hemisphere at $x = 8.5R_E$, $y = 0.8R_E$, and $z = -1R_E$.

at 38:00 (FTE3) and 42:00 (FTE4) into simulation. In this case the normal magnetic field B_N in both events first points inward (− negative) as the structure approaches the probe and then outward (+ positive) as it departs. This polarity is called "reverse" (−/+) (Rijnbeek et al., 1982), and it is associated with FTEs located south of the equator. Therefore, our observation of the simulated bipolar signatures is in agreement with previous observations: "direct" in the Northern Hemisphere and "reverse" in the Southern Hemisphere. The bipolar signature of FTEs are "direct" or "reverse" depending if the probe (or spacecraft) is located north or south, respectively, to the X reconnection line.

We observe intensifications of the B_M component during these FTE events. The middle plot of Figure 3a (Northern Hemisphere) shows a clear enhancement of the B_M component (core magnetic field) related to the bipolar signatures observed at times 29:00 and 40:00. There is also an increase of the B_M component associated with FTE2 at 32:00. In the same way, associated with the second bipolar signature of Figure 3b (FTE5 in Southern Hemisphere), there is a very clear increase of the B_M component at ∼42:00. This is not the case for FTE3 at about 38:00, where the intensification of the core magnetic field is not very obvious.

The third panels of Figures 3a and 3b show when the magnetopause moves outward and crosses the virtual probe. The crossing is defined as the moment when $B_L = 0$.
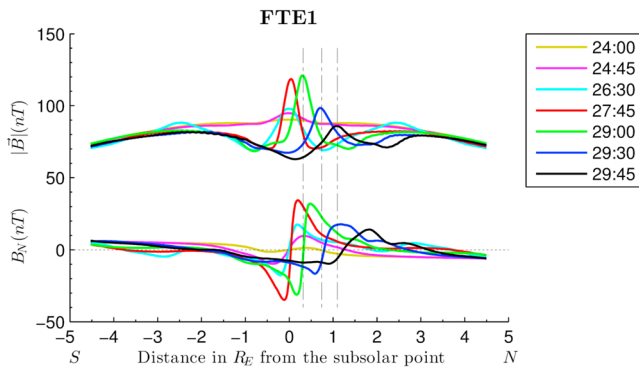
Figure 4. Plots of the normal component of the magnetic field (bottom) and total magnetic field strength (top) for the time interval from 24:00 to 29:45. The x axis corresponds to the length of the trajectory of the Shue et al. (1997) magnetopause model, taken as reference the subsolar point. Negative and positive values indicate that the measures were taken in the Southern and Northern Hemispheres, respectively, along the trajectory. Each color means a specific time run. The vertical dashed lines indicate the position of maximum peaks of the total magnetic field for the last three times.

In summary, we detected five well-formed FTEs. Three of them were observed only in the Northern Hemisphere (FTE1, FTE2, and FTE4). The other two FTEs were detected only in the Southern Hemisphere (FTE3 and FTE5). The numbers are given according to their sequence in time.

The FTE signatures are detected only when the structure pass through the single virtual satellites, which is some time after its formation. Therefore, we use the multiple satellite technique outlined in the methodology to identify accurately the onset time of every event. The evolution of FTE1 is shown in Figure 4. The bipolar signature in B_N was first detected at 24:00 (yellow line at the bottom plot). It starts to grow at the magnetopause subsolar point up to a value of $B_N = \pm 35$ nT or 70 nT peak to peak, which is considered a high value (see red line of B_N). From 24:00 to 27:45 the FTE1 does not move from the subsolar point. Figure 4 (red and green lines at the top plot) shows a strong intensification of the total magnetic field (B_T) from ~ 60 nT up to ~ 120 nT occurs at the center of the event. This increase of B_T is directly related to an intensification of the core magnetic field relative to the ambient magnetic field by the ratio: $\delta B = \left(\frac{B_{Tcenter}}{B_{Tambient}} \right) \approx 2$.

At about 27:45 the bipolar signature and the peak of the magnetic field magnitude start to move to the north (positive in the x axis). Also, the strength of both the bipolar signature and the total magnetic field at the center begins to decrease as the structure moves away from the subsolar point.

The FTE1 propagation velocity is calculated between the times 29:30 and 29:45. The peaks of total magnetic field magnitude are taken as reference points for the center of the structure. The propagation velocity of the structure is ~ 150 km/s, which is consistent with observations (e.g., Fear et al., 2007). The angle of propagation is approximately 30° counterclockwise taken as reference the positive Z GSM axis, that is, the direction of its motion is northward and downward.

Using the same methodology, we identify the following parameters for every FTE in the simulation: exact time of formation, their lifetime in minutes, the magnitude of their bipolar signature, the relative increase of the total magnetic field at the center of the FTE respect to surrounding magnetic field, when they start to move, if they move toward North or South, and the speed of propagation. The characteristics of the events analyzed in this section are summarized in Table 1.

3.1. Generation and Topology of IFTs Associated With FTE1

After 24:00 the subsolar magnetopause becomes very unsteady with the occurrence of five well-formed FTEs with significant magnetic signatures. This time can be considered as a breakpoint in the stability and symmetry of the subsolar magnetopause. Throughout this section we analyze the mechanism of generation of FTE1 and we will show that it is not a normal FTE; instead, it is formed by two IFTs with the typical characteristic of an FTE.

Table 1
Summary of the Characteristics of the FTEs Observed in our Simulation

|	FTE1	FTE2	FTE3	FTE4	FTE5
Bipolar B_N start time	24:00	31:30	37:15	39:00	41:45
Bipolar B_N end time	30:00	34:30	38:45	43:00	43:00
Duration time of the bipolar signature peak to peak	6 min	3 min	1 min 30 s	4 min	1 min 15 s
Magnitude of the bipolar signature peak to peak	70 nT	27 nT	29 nT	100 nT	20 nT
$\delta B = \left(\frac{B_{Tcenter}}{B_{ambient}} \right)$	2.0	1.4	1.85	2.4	1.1
Direction of propagation, North (N) or South (S)	N	N	S	N	S
Time of movement start	28:00	31:30	37:15	40:30	42:15
Speed of propagation (km/s)	150	102	229	135	182

Note. FTE = flux transfer event.
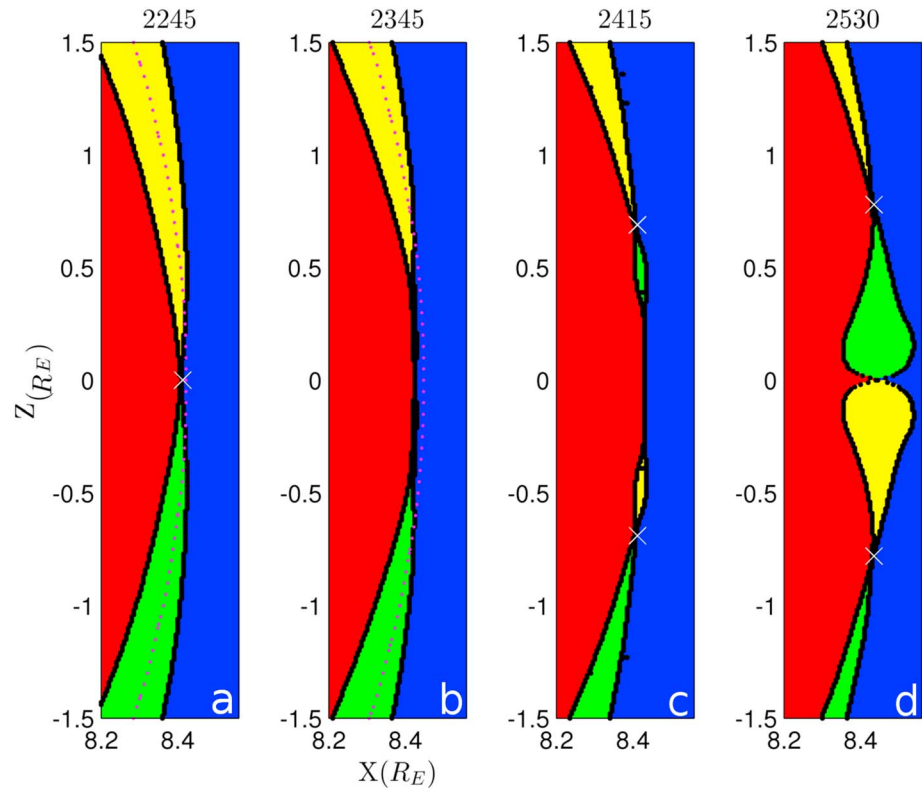
Figure 5. Change of the magnetic topology for the noon-midnight plane ($Y = 0\ R_E$ plane) for different times. The colors represent the magnetic topology as red, closed; green, one end connected to the south and the other open; yellow, one end connected to the north and the other open; and blue, IMF lines. The white cross markers show likely reconnection points. The dotted magenta line indicates the intersection of the isosurface of $B_Z = 0$ with the noon-midnight plane.

We have analyzed the magnetic topology of the first FTE observed in our simulation, which is shown in Figure 5. The following color classification to the points in Figure 5 (and Figure 6) is given:

1. red if the point belong to a closed (dipolar) magnetic field line;
2. yellow if the point belongs to magnetic lines with one end in the Northern Polar Cap and the other end in the interplanetary space;
3. green if the point belongs to magnetic lines with one end in the Southern Polar Cap and the other end in the interplanetary space;
4. blue if the point belongs to an IMF line.

Figures 5a and 5b show that at about 23:45 the magnetic topology starts to change. First, at 22:45 an X-point type separating the four different topology regions is observed at the center of Figure 5a (see white cross marker). At the time 23:45 the X-point has disappeared, that is, there is no a point where the four topology regions meet. Instead there are two Y type points at $Z = \pm 0.5\ R_E$ where three topology regions meet (yellow, red and blue at $0.5 R_E$ and green, red and blue at $-0.5 R_E$). The two Y points are joined by a line that separates the closed (red) and IMF (blue) topological regions.

Starting from the time 24:15, the two Y points become X-points. In the Northern Hemisphere at $\sim 0.75\ R_E$ (see Figures 5c and 5d), reconnection produces field lines connected to the Southern and Northern Hemisphere. Similarly, in the Southern Hemisphere magnetic reconnection at $\sim -0.75\ R_E$ produces field lines connected to each hemisphere. As result of the reconnection at this two points, a structure of semiopen magnetic field lines connected to Southern Hemisphere has been formed in the Northern Hemisphere (green lobe of Figure 5d) and a structure of semiopen magnetic field lines connected to Northern Hemisphere has been developed in the Southern Hemisphere (yellow lobe of Figure 5d).

Figures 6a–6d show the magnetic topology on a surface very close to the magnetopause. The surface is calculated as an isosurface of $B_Z = 0$, which is a very good approximation of the subsolar magnetopause for our
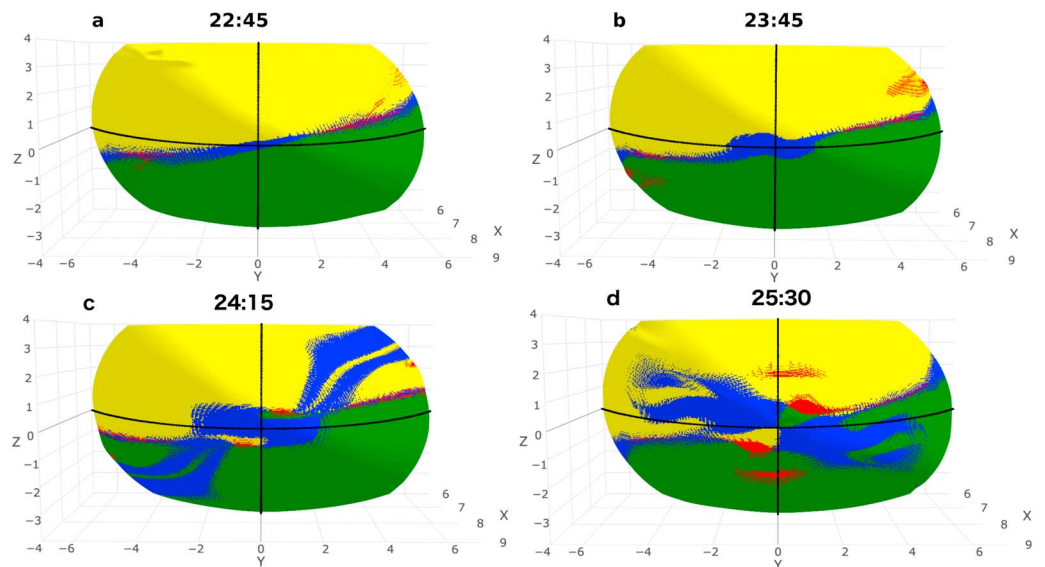
Figure 6. Magnetic field topology over an isosurface of $B_Z = 0$ nT. The surface is very close to the magnetopause but in the magnetosheath side. The colors represent the magnetic topology as red, closed; green, one end connected to the south and the other open; yellow, one end connected to the north and the other open; and blue, IMF lines. The black lines show the intersection of the isosurface with the $Y = 0R_E$ and $Z = 0R_E$ planes. The view is from the north dawnward sun side.

simulation with the IMF southward and duskward. For every point of the isosurface we trace the magnetic field line that belongs to this point and calculate its topology.

We observe in Figure 6a that the magnetopause is separated into two principal topological regions: one in the top half with field lines connected to the Northern Polar Cap (yellow region) and the other one in the bottom half with field lines connected to the Southern Polar Cap (green region). The two regions are separated by a thick blue line which represents a region of IMF lines. Figure 5 shows the magnetic topology in the noon-midnight plane ($Y = 0$ cut) for the different times, where the classification of the regions is the same. The dotted line of the first and second panel indicates the intercept of the isosurface of $B_Z = 0$ at 22:45 and 23:45, respectively. A comparison between Figures 6a and 5a reveals that the thick blue line is very close to the interception point of the four topological regions where magnetic reconnection occurs. Therefore, the blue band in Figure 6a is a very good approximation of the reconnection X-line through the magnetopause.

We have calculated the inclination of the reconnection X-line identified by the topology method. The angle between the projection of the X-line over a plane YZ and the equatorial plane is $\approx 13°$. This tilt of the X-line is expected according to the component merging model (e.g., Gonzalez & Mozer, 1974; Sonnerup, 1974) and is consistent with spacecraft observations (e.g., Trenchi et al., 2008).

Figure 6 shows how the change of topology affects the reconnection line. From the beginning of the simulation up to 22:45 (Figure 6a) the magnetic topology does not change; consequently, we consider it is steady until this time. At the time 23:45 (Figure 6b) the reconnection site at the magnetopause is no longer an extended line. In the subsolar region the IMF magnetic field starts to accumulate producing a deformation of the reconnection line. Comparing the two images it can be seen that the change of topology is restricted to $Y \approx \pm 1.5 R_E$, $Z \approx \pm 1 R_E$; therefore, outside this region the magnetic reconnection process keeps steady along the same X-reconnection line.

Figures 6c and 6d show the increasing accumulation of IMF lines and the emergence of new topology regions at the subsolar magnetopause, specifically in the northward and duskward and southward and downward sector. The creation of these new topology regions is a direct consequence of magnetic reconnection at the two reconnection lines created northward and southward the subsolar point.

The effects of this IMF accumulation on the subsolar magnetic field are shown in Figure 7. The green arrows represent the direction (not the magnitude) of the projected magnetic field over the noon-midnight plane, the blue lines are streamlines of the projected magnetic field, and the color code represents the thermal pressure.
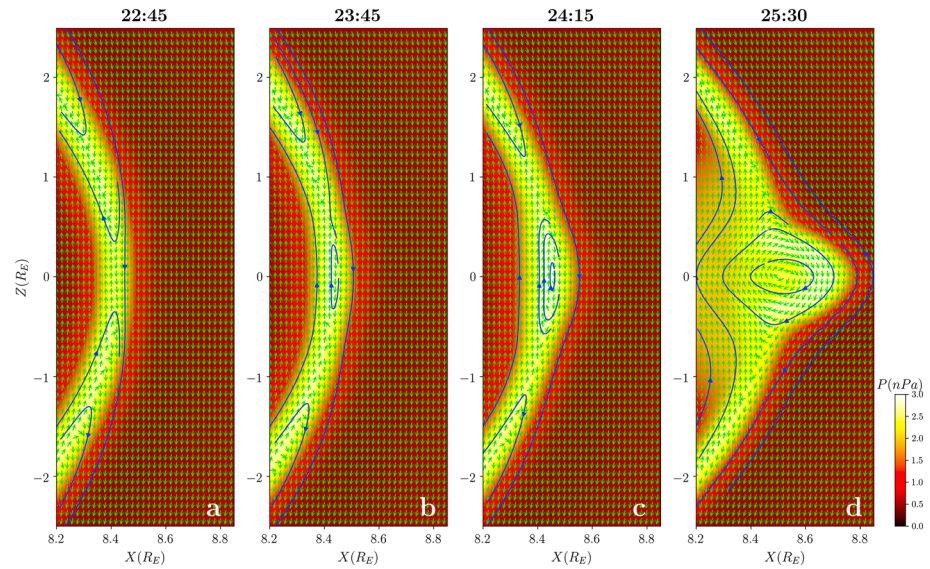
Figure 7. Formation of the IFTs for the noon-midnight plane. The plasma thermal pressure is shown in color code. The green arrows indicate the projection of the magnetic field on the *X-Z* plane. The blue lines are projected magnetic field lines.

The accumulation of IMF at the subsolar magnetopause, shown in Figures 6 and 5, causes a bending of the magnetic field in this region and as consequence the creation of an "O" type point at the center of the bulge. At 22:45 (Figure 7a) the projected magnetic field is purely southward at the subsolar point; however, at 23:45 (Figure 7b) a slight curvature of the magnetic field can be observed jointly with the formation of a magnetic loop. This is the time when the IMF starts to accumulate at the subsolar point. The curvature or bending is more pronounced at subsequent times. At about $\pm 0.75\ R_E$ in Figures 7c and 7d the formation of two X-points at the edges of the "O" shape structure can be observed (similar to the tearing instability). To confirm that these X-points of the projected magnetic field are actually reconnection points, we look at Figure 5 at 24:15. It can be observed that approximately in the same area ($\pm 0.75\ R_E$) there are two points where the four topology regions meet (white cross symbols). Thus, two reconnection places have been formed in the Northern and Southern Hemispheres.
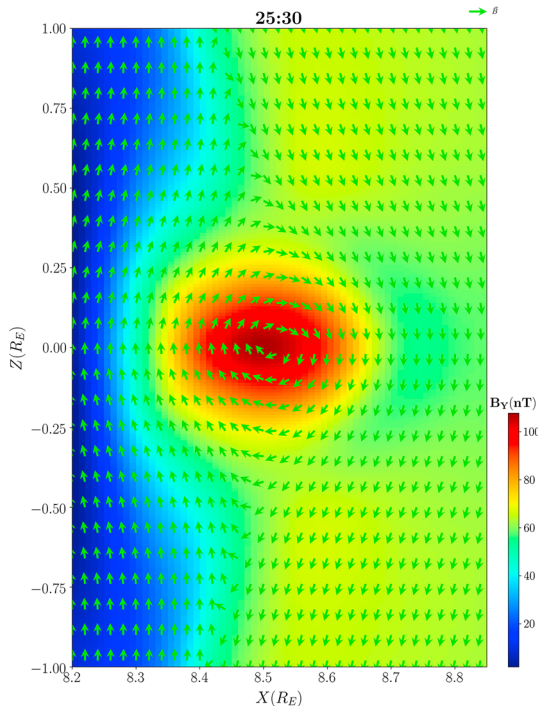
Figure 7d shows a pressure bulge of $\sim 1\ R_E$ extent in the *Z* direction. However, the most important aspect in this figure is that the projected magnetic field has the characteristics of a magnetic flux rope (e.g., Sonnerup, 1988): first, a clear rotation of the magnetic field in two dimension is observed, which is characterized by the formation of an "O" neutral point (see white lines and green arrows at the center of the FTE); second, a large core magnetic field characterized by a large out-of-plane magnetic field component of about 100 nT is present (see Figure 8 where the B_Y component is shown in color code). As we will show soon this structure is not a flux rope.

The analysis of the projected magnetic field, in conjunction with the topology study, gives a correct understanding of the magnetic structure. However, if we use only the projected magnetic field we may get an erroneous interpretation of the FTE magnetic configuration (Dorelli & Bhattacharjee, 2009).

Figure 8. The color code represents the *Y* component of the magnetic field. The green arrows indicate the projection of the magnetic field on the *X-Z* plane. The magnetic structure is well formed with a rotational magnetic field and an intensification of the core magnetic field.

Looking at Figures 7d and 8, we observe a good similarity with the 2-D reconstruction of a flux rope using Cluster spacecraft (e.g., Sonnerup et al., 2004, Figure 2). The flux rope reconstructed in that paper shows a strong core magnetic field in the axial (out-of-plane) direction similar to that
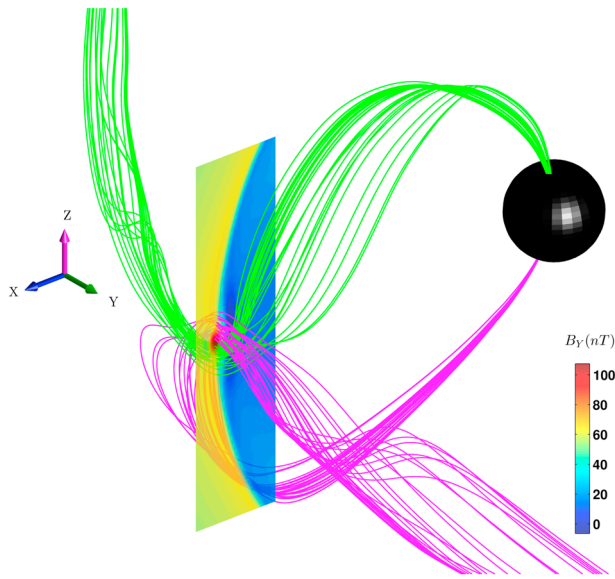
Figure 9. Three-dimensional perspective of the interlinked flux tubes. The view is from the north duskward direction. The radius of the black sphere is 3 R_E, which is concentric with Earth and represents the inner magnetosphere. The color coded plane shows the intensity of the Y component of the magnetic field for the noon-midnight cut.

found in Figure 8. There is also a pressure bulge of ~1 R_E size. In their case the thermal pressure is higher at the edges of the FTE than at the center, to keep the total pressure (thermal + magnetic pressure) almost constant. In Figure 7d this pressure bulge is quite evident; also, the thermal pressure is higher at the edges than at the center, indicating the existence of a force balance between the magnetic and thermal pressure. The last clue that moved us to identify this structure as a single flux rope is the rotation in the projected magnetic field, which is found typically in a cross-section view of the flux rope. This rotation of the magnetic field is responsible for the bipolar B_N signature shown in Figure 4. A spacecraft that transverses the FTE from north to south(south to north) sees first a magnetic field outward (inward) normal to the magnetopause and later an inward (outward) B_N component.

A clear 3-D view of this event at 25:30 is shown in Figure 9. Two IFTs with an elbow-like structure can be distinguished. One of them has one side connected to the Northern Polar Cap and the other side open (green lines). The second flux tube has one side connected to the Southern Polar Cap and the other side open (magenta lines). The peculiarity lies in that the two flux tubes are interlinked, then when these flux tubes convect to the tail, they are forced to move against each other. The B_Y component of the magnetic field is presented in color code for a meridional cut ($Y = 0$ R_E) centered at the subsolar magnetopause. An intensification of the B_Y magnetic field component is observed in the region where the two flux tubes meet. This region is very close to the subsolar point; hence, the B_Y component can be considered a good approximation of the B_M component of the boundary normal system.

From Figure 9 we deduce that the rotational magnetic field is not due to a flux rope; instead, it is because of the linkage of two IFTs. In the region where the two tubes intercept, they exert magnetic tension against each other, which produces a bending of the magnetic field and an enhancement of the core magnetic field in the region where the tubes meet.

The magnetopause can be approximately identified in the noon-midnight cut of Figure 9, as the separation line between blue ($B_Y \approx 0$ nT) and yellow ($B_Y > 0$ nT) color regions. The direction of the magnetic field of the southern connected (magenta) flux tube points from the magnetospheric side to the magnetosheath side, that is, outward (+) from the magnetosphere. On the contrary, the magnetic field direction of the northern connected (green) flux tube points inward (−) to the magnetosphere. When the two flux tubes are projected in the noon-midnight plane, the rotational magnetic field of Figure 8 is reproduced. Therefore, the signatures of the FTE1 are caused by the IFTs and not by a single flux rope. Also, it is observed from the projected magnetic field and the line plot of Figure 4 that each tube independently does not produce the bipolar signature of B_N, which means that the magnetic field in each tube is not twisted (Cardoso et al., 2013). This explains the single bipolar signature observed during this event.

The evolution of the IFTs is shown in Figure 10 in terms of plasma pressure. In Figure 10a the IFTs are well formed and stationary. Two possible reconnection points can be identified at this time at ~$z = \pm1.4$ R_E, due to bidirectional flow speeds observed around this points. The observation of the reconnection points north and south of the subsolar magnetopause is consistent with the results of the magnetic topological study, which also reveals the existence of X points in the same region where the four topology zones meet. If we observe carefully Figure 5d, the subsolar point is also a meeting point of the four topology regions. However, from Figure 10a it is shown that plasma is accumulated in this region due to it is being ejected from the reconnection points to the center of the FTE. Hence, as the flow is converging at the subsolar magnetopause instead of diverging, reconnection has probably been suppressed in this region as pointed out by Cardoso et al. (2013). The accumulation of the plasma coming from the reconnection points to the center is the cause of the big pressure bulge shown in Figure 10a at 26:30. The most probable reconnection sites are located at the junctions of the four topological regions. As this is a necessary but not a sufficient condition, it would not be contradictory if the four-field topological junction was not a reconnection point, however.
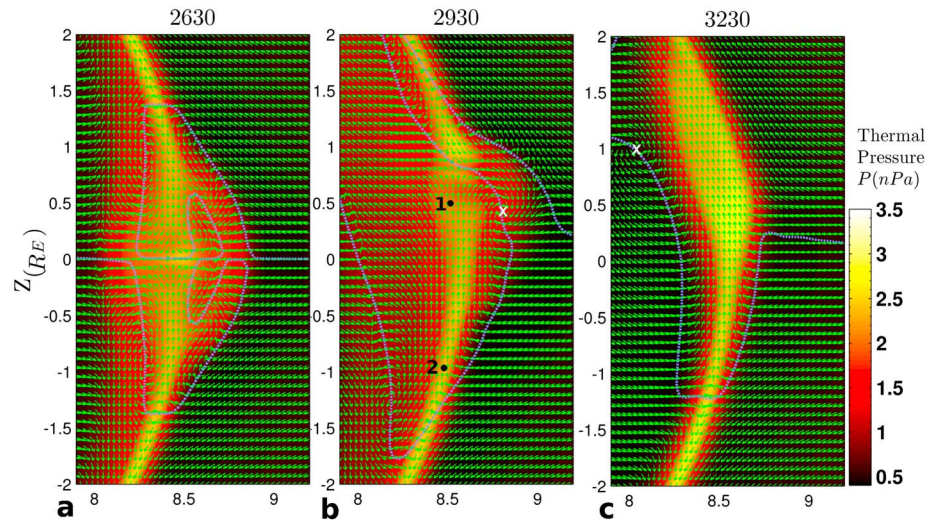
Figure 10. The three panels show cuts of the noon-midnight meridional plane at different times. In each panel the color coding indicates the thermal pressure. The green arrows indicate the direction (not the magnitude) of the projected bulk plasma velocity vector, in order to emphasize the flow vortices represented by the white cross symbols. The thin dotted blue line is the zero contour of the plasma velocity Z component; that is, it separates regions of $V_Z > 0$ from regions of $V_Z < 0$. The white cross markers show the flow vortices centers. The black points indicate the location where the plasma velocity has been collected.

Figure 10b shows a snapshot of the IFTs when the pressure bulge has moved northward from the subsolar point at the time 29:30. We measure the plasma flow speed at two different points: one at the center of the IFTs (point 1 in Figure 10b) and the other outside the structure in the magnetopause current sheet (point 2 in Figure 10b), slightly northward from the reconnection point located around $-1.5\ R_E$. We compare these values with the IFTs' propagation velocity calculated at the end of section 3. We found out that the following relation is reasonably well satisfied:

$$\vec{V}_1 = \vec{V}_2 + \vec{V}_{\text{IFT}}, \tag{2}$$

where $\vec{V}_1$ is the plasma velocity vector measured at point 1, $\vec{V}_2$ is the plasma velocity vector measured at point 2, and $\vec{V}_{\text{IFT}}$ is the IFTs propagation velocity calculated in section 3 using position timing. In GSM coordinate system $\vec{V}_1 = (-3, -100, 231)$ km/s, $\vec{V}_2 = (-5, -22, 94)$ km/s, and $\vec{V}_{\text{IFT}} = (0, -75, 130)$ km/s. Equation (2) means that the plasma flow inside the IFTs can be a superposition of the IFTs propagation velocity and the outflow velocity coming out from the reconnection site formed southward the subsolar point.

We also calculated the velocity of the IFTs in the deHoffman-Teller frame (Cowley & Owen, 1989) and compared it with the IFTs propagation velocity, but the results were not satisfactory. The propagation velocity is far smaller than the deHoffman-Teller velocity. The discrepancy can be explained as following. The deHoffman-Teller velocity is calculated based on the assumption that during typical conditions the magnetospheric plasma has negligible dynamical significance in the stress balance relation across the magnetopause (Cowley & Owen, 1989); this is due to expectations that the plasma density in the magnetosphere is generally much less than on the magnetosheath side. For our simulation conditions (large IMF B_Z and B_Y components) this is not the case, in fact the magnetosheath is not well compressed and the magnetospheric plasma density is comparable in magnitude to the magnetosheath plasma density.

As it is noted above in Figure 6, the topology at the magnetopause around $\pm 1.5\ R_E$ changes and becomes unsteady near 24:00. However, after and during the decay of FTE1 the magnetic topology at the magnetopause becomes even more complex and the complexity extends to a wider area of the subsolar magnetopause (about $\pm 6\ R_E$ in Y and $\pm 4\ R_E$ in Z directions). We observe the creation and destruction of regions of different magnetic topology until the end of the run. Therefore, the magnetic reconnection process is far from being a quasi-steady process along a reconnection line. Due to this unstable behavior, the reconnection locations are difficult to identify by topological methods. We use the $V_Z = 0$ contour lines and the flow speed to estimate where reconnection is happening. The $V_Z = 0$ contour line is represented as a blue dotted line in Figure 10. We can define this line as a "stagnation" line in the sense that it separates regions of northward

flow from regions of southward flow; hence, the interception of the contour line with the magnetopause is n stagnation point (Raeder, 2006).

One important result from Figure 10 is the shift of the stagnation points from the subsolar point. At the time 26:30 two stagnation points are detected at $Z \approx \pm 1.4\, R_E$ (see interception of the $V_Z = 0$ line with the magnetopause); in this case these stagnation points are directly associated with magnetic reconnection near that region. Plasma ejected from the stagnation points increase the thermal pressure inside the IFTs. The flow pattern is almost symmetric with respect to the x axis at that time. There is a balance of force between the gradient pressure and the magnetic force that keeps the symmetry. The pressure bulge grows until the balance of forces, and symmetry is broken. After that moment the structure begins to move northward. Figure 10b shows a snapshot of the IFTs when is moving northward. The northern stagnation point has moved northward (out of Figure 10b), and the southward point remained almost in the same place. As result, after the IFTs start to move, only one stagnation point (and possible reconnection point) remains southward to the equator. The subsequent FTE in Figure 10c moves northward because it has been formed northward to the remaining reconnection point located at $Z \approx -1.4\, R_E$.

The shift of the stagnation point from the subsolar magnetopause was also reported by Raeder (2006). In that case the shift was caused by a large dipole tilt of 34° toward the Sun during summer solstice. For this configuration of the magnetic dipole, the nose of the magnetopause (defined as zero magnetic latitude) is located southward the Sun-Earth line (x axis). This causes a displacement of both the X-line and the stagnation point more southward, following the position of the magnetic equator, where the local magnetic shear is maximum. We use no dipole tilt, which means that the subsolar-stagnation point is located at the Sun-Earth line (at least until 24:00); that is, there is a north-south symmetry. Therefore, in our run the stagnation point moves from the subsolar point as a result of the instability. Raeder (2006) also runs a simulation for no dipole tilt but purely southward IMF ($B_Y = 0$); for this case steady reconnection occurs at the magnetopause. This suggests that the B_Y component is important to break the symmetry at the magnetopause and produce nonsteady reconnection as observed in our simulations.

Another interesting result is the formation of flow vortices. Inspection of the 29:30 and 32:30 snapshots in Figures 10b and 10c shows that the center of the flow vortices, represented by white x symbols, is intercepted by the contour line of $V_Z = 0$. The $V_Z = 0$ contour line is a boundary between regions of opposite orientation in the Z component of the plasma velocity; hence, there is a flow shear in the proximity of this line that can generate the observed flow vortices. Dorelli and Bhattacharjee (2009) using OpenGGCM (Open Geospace General Circulation Model) also detected flow vortices in their simulations and showed that the flow vortices bring together regions of different magnetic topology which drive more processes of magnetic reconnection. We believe that the increase of the complexity of the magnetic topology, after the IFTs have formed and propagated (not shown), could be due to magnetic reconnection driven by the flow vortices after the IFTs have been formed.

3.2. Creation of Multiple X-Reconnection Lines

We now go back to the question about the causes of the instability in the subsolar magnetopause starting at 24:00. We have mentioned the generation mechanism of the IFT that is responsible for breaking the stability of the magnetopause. Here we provide further details.

Figure 11 shows a sequence of snapshots of the stagnation line (black dotted line) over the magnetopause. This is the line that divides flows of $V_Z > 0$ km/s (toward north) from flows of $V_Z < 0$ km/s (toward south). The Z GSM component of the plasma velocity is measured in every point of the surface and showed in color code.

At 23:30 (Figure 11a) the stagnation line matches very well with the reconnection line calculated using the topology method. The inclination angle is the same ($\approx 13°$). At 24:00 (Figure 11b) we start to observe a stagnation line that is modified from its initial extended only line form. After 24:00 the stagnation line still intersects the subsolar point; however, at $0.3 R_E$ dawnward and duskward, the stagnation line has been shifted northward and southward, respectively. As time goes on, the shift grows in the Z direction up to $\sim \pm 3\, R_E$ and remains approximately steady until the final stage of the IFTs. A more advanced snapshot at 25:15 (Figure 11d) shows that the stagnation line has a "S" shape near the subsolar region.

If we consider the stagnation line as approximate location for the reconnection line, we can identify the formation of two reconnection lines, northward and southward the subsolar point, of $\approx 2\, R_E$ of longitudinal extension. At 25:15 we observe a southward (northward) directed flow of about 100 km/s coming
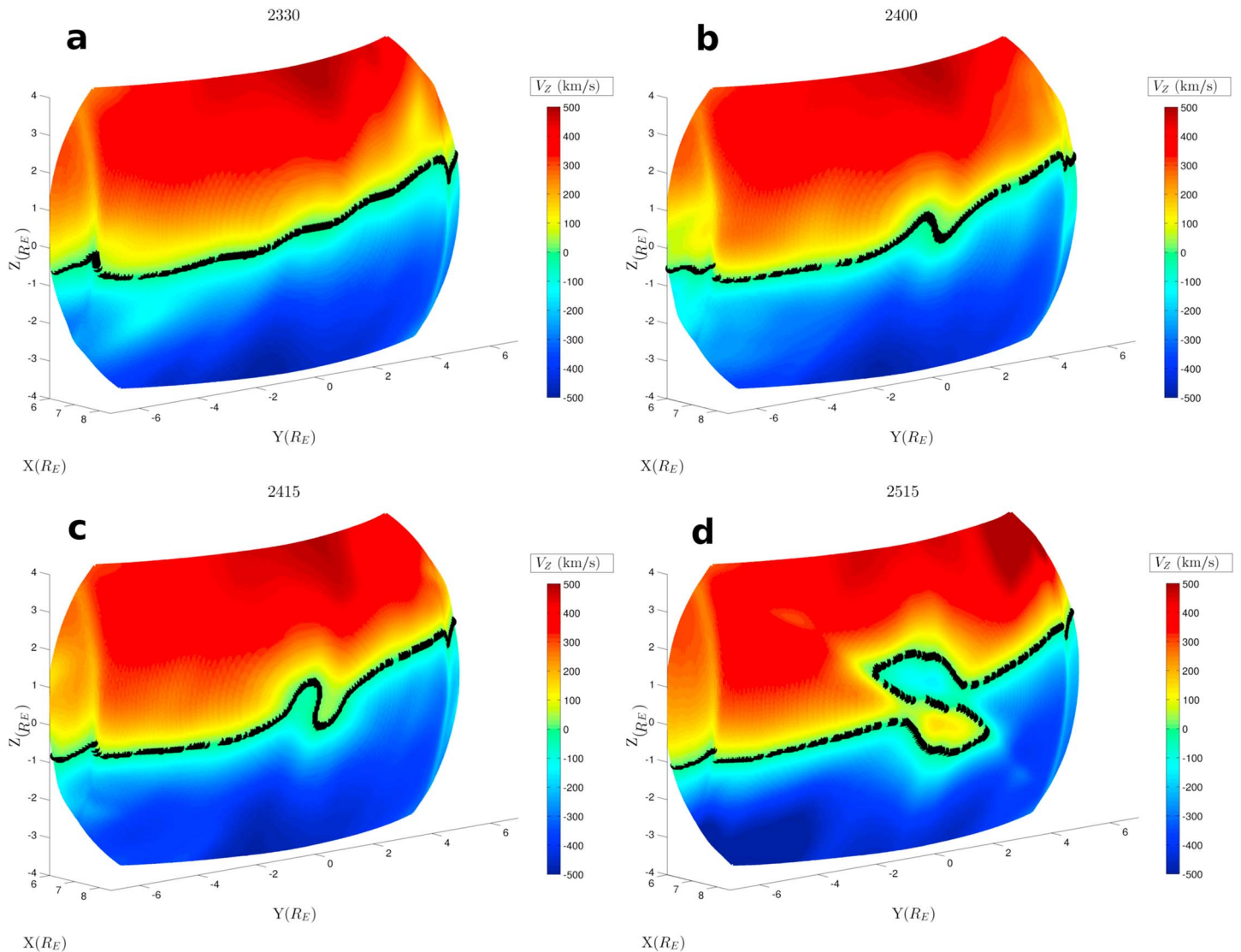
Figure 11. Sequence of the subsolar magnetopause plots seen from the magnetosheath side for different times. The color coding represents the Z component of the plasma velocity over an isosurface of $B_Z = 0$ (magnetopause). The black line represents the stagnation ($V_Z = 0$) line.

from the northern (southern) reconnection line. Despite the subsolar point is a stagnation point (in the sense of $V_Z = 0$), we do not believe that it is a reconnection site, because in the subsolar region these flows converge instead of diverging.

Figure 12 shows the evolution of the magnetic field component normal to the magnetopause (left column) and the tangential component (right column). These quantities are calculated at the magnetopause (isosurface of $B_Z = 0$) for $\pm 2\ R_E$ in the Y and Z directions. The magnetic reconnection process is more likely in regions of low tangential magnetic field. This condition follows because the tangential components of the magnetic field perpendicular to the X-line on either side of the magnetopause are antiparallel; therefore, when they meet at the X-line, the overall magnitude of the tangential field to the magnetopause is reduced. On the contrary, from Figure 12 (right panel) we observe an increase of tangential magnetic field near the subsolar point, indicating that magnetic reconnection is indeed suppressed in that region. Simultaneously to the accumulation of the tangential magnetic field, an increase of the normal component at the peaks of the stagnation line is observed (see Figure 12, left column). These are typical signatures of the resistive tearing mode. For example, in 2-D simulations (i.e., Ding et al., 1991), the normal component of the magnetic field has opposite directions at the edges of the plasmoid (X-points). In 3-D simulations a plasmoid still forms in terms of density and thermal pressure (see Figure 7b). However, there is no formation of magnetic islands
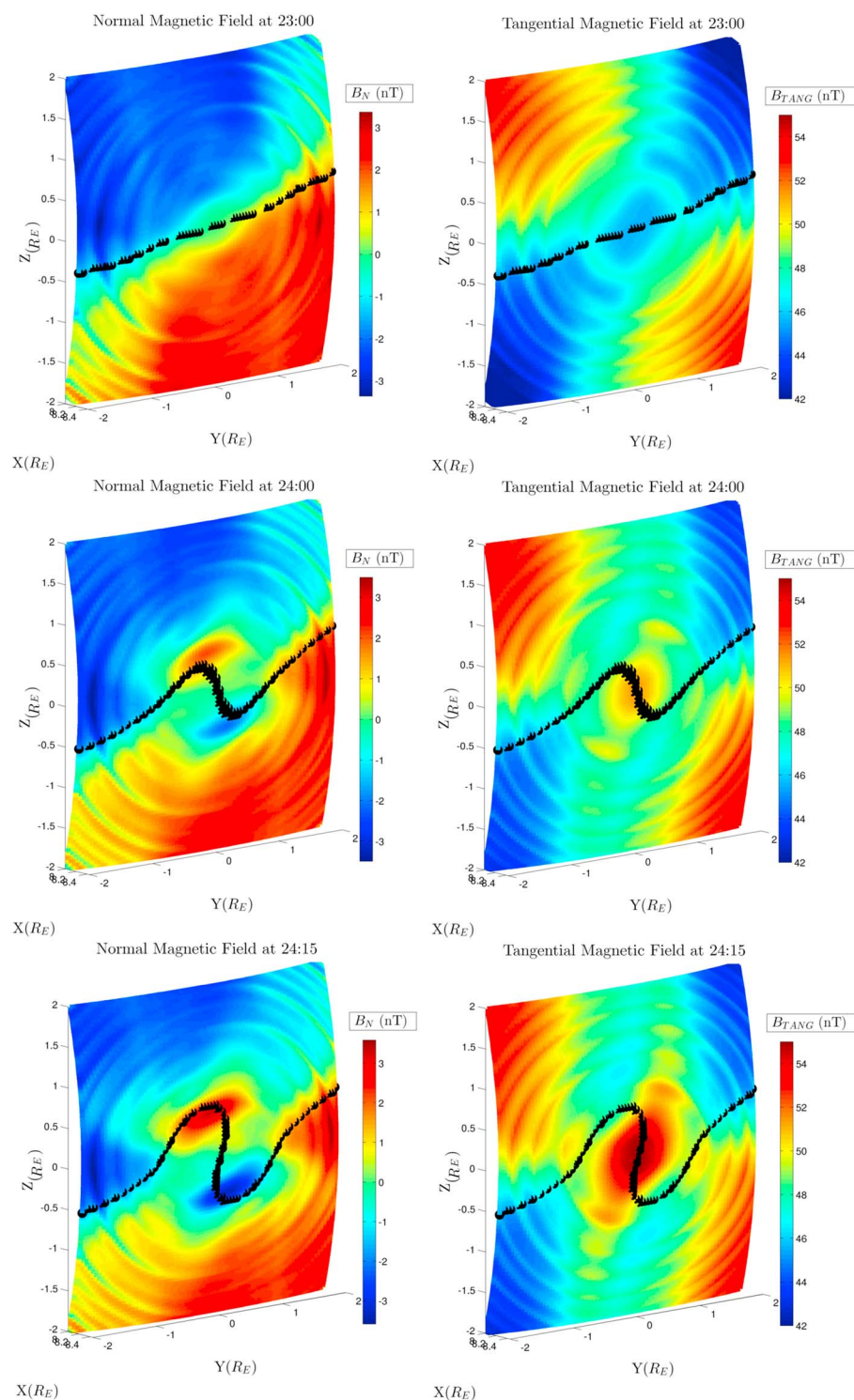
Figure 12. Sequence of the subsolar magnetopause plots seen from the magnetosheath side for different times. The left column shows the normal component of the magnetic field over an isosurface of $B_Z = 0$. The right column shows the tangential component of the magnetic field to the magnetopause. The black line represents the stagnation ($V_Z = 0$) line.
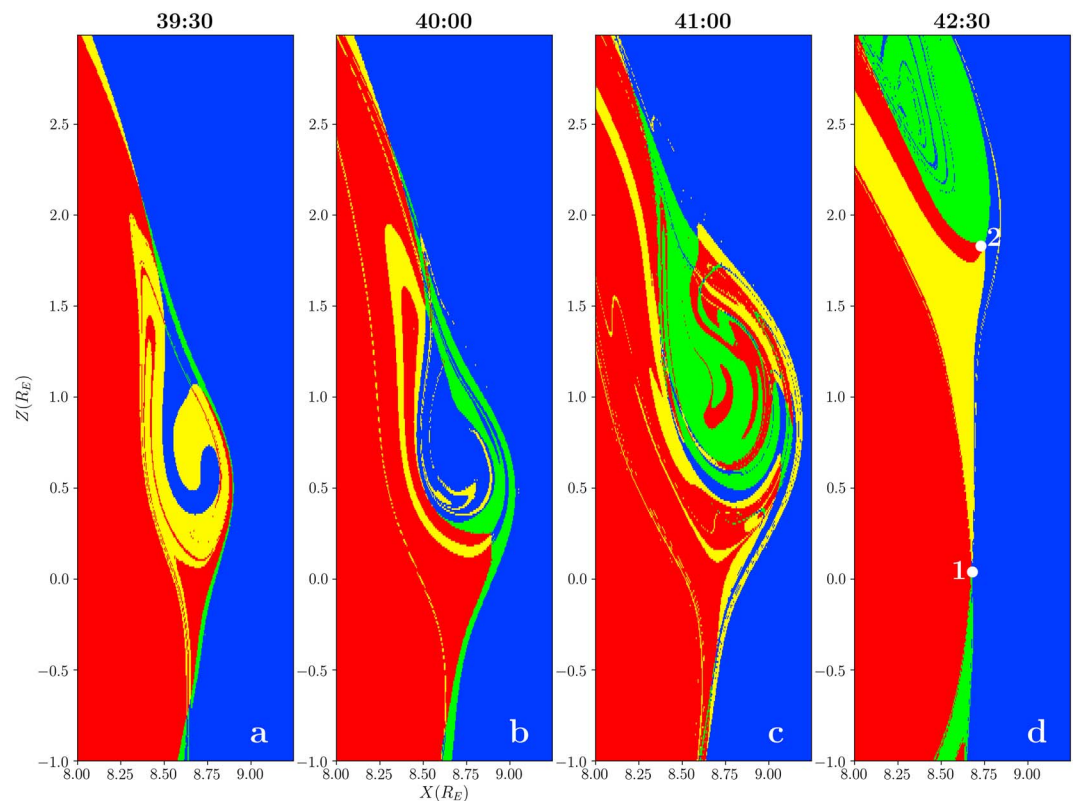
Figure 13. Flux transfer events 4 magnetic topology for the noon-midnight plane ($Y = 0\ R_E$ plane) for different times. The colors represent the magnetic topology as red, closed; green, one end connected to the south and the other open; yellow, one end connected to the north and the other open; and blue, IMF lines. The white markers show likely reconnection points.

as in the 2-D case because of the presence of the B_Y component. The curved magnetic field lines at the edges wrap and compress the core magnetic field lines at the center of the structure, which produce an increase of the tangential magnetic component.

3.3. Generation and Topology of IFTs Associated With FTE4

In the preceding sections we have analyzed in great detail the FTE1 and its associated IFTs structure. Now we move forward and look for similar structures in the others FTE detected in our simulation. This will give us a sense of how likely the IFTs are formed and more information about its mechanism of formation.

We searched for magnetic field topologies similar to that for FTE1. During the time interval of every FTE we look for regions of north (south) connected magnetic field southward (northward) from the reconnection point, because this kind of topological structure is more likely to result in magnetic IFTs like the ones found in FTE1. Of all the subsequent FTEs following FTE1, the only that presented an IFTs structure was FTE4; however, we found that its mechanism of formation and topology is different than for the FTE1. The sequence of events that lead to the formation of IFTs in this FTE will be described in this section.

Figure 13 shows the magnetic topology of FTE4 in the $Y = 0\ R_E$ plane for different times ranging from first development to the end of the bipolar FTE4 signature (see Table 1). Figure 13a shows the formation of vortex like topology regions of open magnetic field lines connected to the Northern Hemisphere (yellow regions). This spiral vortex formation is characteristic of twisted magnetic field lines inside the FTE. Figure 14a shows a 3-D perspective of the magnetic lines crossing the core of the FTE. The magnetic field lines (mainly north connected and IMF) are highly twisted, which indicates that this event is a typical flux rope unlike FTE1.

The twisted magnetic field lines bring together regions of opposite magnetic directions (northward and southward), creating favorable conditions for magnetic reconnection and changes in the magnetic topology. Figure 13b shows the formation of new regions of open-south connected field lines (green region) at 40:00.
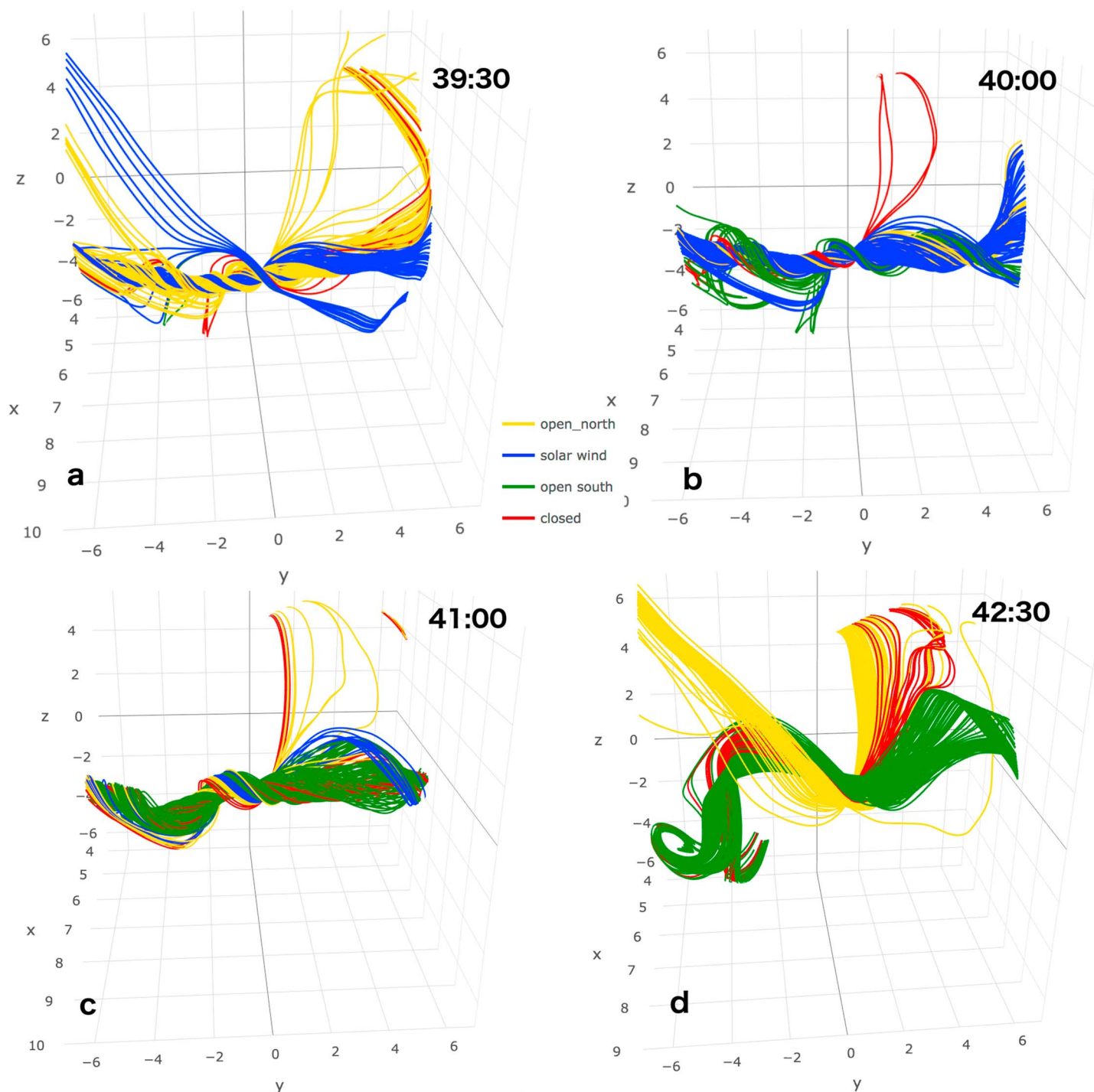
Figure 14. Evolution of the 3-D magnetic structure corresponding to flux transfer event 4. The structure evolves from an initial twisted flux rope configuration to an interlinked flux tubes in d.

At 41:00 the physical size of FTE4 has increased and almost all the magnetic lines of the structure are connected to the Northern Hemisphere (green region).

Figure 13d shows how the topology looks at the final stage of the FTE. We can observe two points where the four topology regions meet, named 1 and 2 (see filled circle markers Figure 13d). We believe that these are reconnection points. The topology shows a green region northward of reconnection point 2 and a yellow region southward of the same point. Although this topology is not symmetric like the FTE1, it could

be an indication of IFTs. Figure 14d shows the 3-D structure of FTE4 at its final stage (42:30). The linkage of magnetic lines connected to Northern Hemisphere (yellow lines) with magnetic lines connected to Southern Hemisphere (green lines) can be observed at this time.

In summary, at its initial stage FTE4 presents a highly twisted magnetic field similar to a classical flux rope. Magnetic reconnection between regions of different topology or directions causes the structure to evolve to a less complex stage as IFTs. We believe that this process indicates a release of magnetic energy stored in the twisted magnetic field as a way to reach a more stable stage. As it is well known, the magnetic helicity in resistive MHD is approximately preserved; this means, at least qualitatively, that the helicity due to the linkages of flux tubes at the final stage accounts for the helicity due to the twisted magnetic field in the first stage, conserving the total magnetic helicity of the structure during the life time interval.

3.4. Role of B_Y in the Generation and Motion of IFTs

In order to test the influence of B_Y on the motion and generation of the IFTs, we carry out a different simulation with the same conditions than in Cardoso et al. (2013) run, only with the exception of B_Y being turned negative this time, that is, $B_Y = -15.81$ nT (downward direction).

Two FTEs have been detected in this new simulation. We observe in the first FTE the formation of IFTs with similar physical and topological properties than the one in FTE1 of Cardoso et al. (2013) run, although the size in the X direction is about 1 R_E (bigger than the first IFTs in Cardoso run). The event originates as an IFTs and remains with this configuration during its approximately 6 min of life. We also observe the same changes in the topology due to the accumulation of IMF at the subsolar point, followed by the grow of the resistive instability and the creation of reconnection sites symmetric positioned respect to the subsolar point. These observations confirm the generation mechanism proposed in section 3.1. The change on the sign of B_Y seems to not affect the symmetry of this kind of IFTs.

Trenchi et al. (2015) suggest that a northward(southward) motion of the X-line is expected for positive(negative) B_Y component of the IMF, according to the sum of the ion and electron diamagnetic drift. Although our simulations are MHD with numerical resistivity, which means that the plasma is considered as a fluid and the effects of the different species are not observed separately, the combined effect of the diamagnetic drift due to electrons an ions is captured in MHD as a diamagnetic current. This current flow points northward(southward) for positive(negative) B_Y. Then, if the motion of the IFTs found in both simulations are indeed influenced by the sign of B_Y, they should move northward(southward) for positive(negative) B_Y. We believe that this effect could be appreciable only when the IFTs present symmetry at the subsolar point, due to the rest of the forces cancel each other.

The IFTs detected in Cardoso run follow this pattern (northward motion for positive B_Y). But in the new simulation for B_Y negative, the IFTs detected do not move neither northward nor southward; that is, they originate, grow, and decay at the subsolar point. We expected a southward motion for this case. Maybe the force associated with the diamagnetic current was not enough to move this big structure. Then, more study is necessary to verify the possibility of B_Y sign being the cause of the northward or southward motion of the IFTs.

4. Discussions and Conclusions

We have analyzed a global MHD simulation run for solar wind-magnetosphere interaction. All the interplanetary conditions have been kept constant during the simulation time. The IMF has a large southward (Z) and duskward (Y) components. The resolution at the subsolar magnetopause is sufficiently high to allow the formation of FTEs.

We observe the spontaneous formation of FTEs under constant solar wind conditions. To study these FTEs, we measure the normal (B_N) and azimuthal (B_M) component along a path very close to the magnetopause. An isosurface of $B_Z = 0$ is used as a reference magnetopause; the normal to the isosurface has been used to build the local boundary coordinate system needed to convert GSM components of the magnetic field to the LMN boundary normal system.

Five FTEs with clear magnetic perturbations were observed after 24:00. The characteristics of these five FTEs are identified: the beginning and end of the magnetic signature, sense of propagation, propagation speed, and the time when they start to move. FTE1, FTE3, and FTE4 traveled northward and downward, while the other two (FTE3 and FTE5) moved southward and duskward. The B_N bipolar signature and the intensification

of the core magnetic field (B_M) were presented in all FTEs, although these signatures were more pronounced in FTE1 and FTE4.

The generation mechanism for the IFTs associated with FTE1 can be summarized as follows. Until about 23:45 reconnection takes place along an extended line with an inclination of $\approx 13°$ with respect to the XY plane when viewed from the Sun. After this time the topology at the subsolar magnetopause changes and the magnetic reconnection switches from quasi-steady to highly dynamic. We identified the source of these topology changes as resulting from an accumulation of IMF at the subsolar magnetopause due to the approach of regions of geomagnetic and IMF lines. At some point the accumulation is faster than the reconnection rate; hence, the concentration of magnetic field saturates the subsolar region and the reconnection is suppressed. The intensified tangential magnetic field enhances the magnetic pressure perpendicular to the subsolar magnetopause, which produces a slight bending of the magnetic field at about 23:45. This time can be considered the beginning of the growth phase for the resistive tearing instability. The bending of the magnetic field favors the creation of new reconnection regions northward and southward of the subsolar point. At 24:15, IFTs start being produced due to the linkage of southern open magnetic lines created at the northward reconnection point and northern open magnetic lines created at the southward reconnection point. The instability continues growing, and the perturbation of the magnetic field increases until an "O"-shaped type point develops. At this moment (25:30) the IFTs are well formed and two new topology regions are well defined.

The cross section of FTE1 has been analyzed in terms of the projected magnetic field, thermal pressure, and core magnetic field. The typical magnetic characteristics of a flux rope are found: a pressure bulge at the center, rotational magnetic field, and a strong core magnetic field. However, the analysis of the magnetic topology reveals that this structure is not a flux rope; instead, it is formed by two IFTs, which together present the same characteristics as a single flux rope. Each IFT separately does not show signatures of an FTE; that is, they are not twisted. This is an example of how a typical study of an FTE without analyzing the magnetic topology leads to an erroneous interpretation of its 3-D magnetic structure.

It is important to highlight that FTE1 develops after originates as an IFTs. For this event, the mechanism for generating the FTE and the IFTs are equivalent because there is only one structure during all the entire lifetime of the event. This implies that IFTs can be considered as another type of 3-D physical structure for FTEs.

The plasma flow inside the IFTs (FTE1) can be considered a superposition of the plasma velocity outside the structure plus the propagation velocity of the IFTs. The deHoffman-Teller velocity does not agree with the propagation velocity of the IFTs. We believe that such discrepancy is because for our simulation conditions, large Z and Y IMF components, there is not a sharp density transition between the magnetosheath and the magnetosphere as it is usually the case.

The magnetic perturbations observed at the subsolar magnetopause during the early stages of the IFTs resemble those for the resistive tearing instability in terms of density, plasma pressure, and magnetic field. Normal magnetic fields with positive and negative polarity have been found northward and southward of the subsolar point, respectively, which indicates the presence of rotational or curved magnetic field lines characteristic of plasmoids. The increase of the tangential field at the center of the structure suggests that magnetic reconnection has been suppressed at the subsolar point. Hence, two new reconnection lines have been created northward and southward the subsolar point. These newly created reconnection lines behaves as stagnation lines where the V_Z flow is zero. They have a limited extent in the Y direction of only about 2 R_E. Thus, as the IFTs associated with FTE1 are formed by these reconnection lines, their dimension depends of the extension of these lines.

We have looked for IFTs in the others FTEs observed in the simulation. IFTs have been found also in the final stage of FTE4. This FTE was generated about 39:00. It presented the typical 2-D signatures of a flux rope like FTE1. The 3-D structure shows that FTE4 is indeed a flux rope with twisted magnetic field lines of different topology. During its evolution the twisted magnetic field lines inside the flux rope change its connectivity, probably due to internal magnetic reconnection between regions of different topology or magnetic orientation. The process continues, but about 1 min before the end of the bipolar signature, the magnetic configuration of FTE4 changes from a flux rope of twisted magnetic fields to an IFTs, within which each tube seems not to be twisted. In this particular event the IFTs result from the evolution of the FTE. Magnetic reconnection may reorganize the connectivity and linkage of the magnetic field lines to a more stable stage. This implies that an FTE with a flux rope configuration may develop into an IFTs at some point during its evolution.

The necessary conditions for an FTE flux rope to evolve to an IFTs remain to be determined. Also, the percentage of twisted lines that becomes interlinked is unknown.

There are some differences between the IFTs observed in FTE1 and FTE4. In the former, the FTE originates as an IFTs and remains with this configuration until its end. Previous to the IFTs formation, in FTE1 the X-line follows the Gonzalez and Mozer (1974) model location. IFTs form due to two reconnection lines positioned symmetric with respect to the subsolar point. Therefore, this structure must have been generated under symmetric conditions. For the FTE4 case, it develops as a flux rope and changes to an IFTs before it disintegrates. During its formation, reconnection was unsteady and did not follow the Gonzalez and Mozer (1974) model. The two reconnection points found associated with FTE4 are not located symmetrically with respect to the subsolar point. This suggests that the symmetry conditions with respect to the subsolar point prior the formation of the FTE play an important role in the generation of the FTEs as either a normal flux rope or an IFTs.

The validity of the generation mechanism was checked in a new simulation for B_Y negative. We confirm that the observed IFTs follow the same generation mechanism we propose for symmetric type IFTs, like the one in FTE1 of Cardoso run. However, a more detailed study of the balance of forces inside the IFTs will be needed in future works, to understand better the role of B_Y in the motion of IFTs.

References

Berchem, J., & Russell, C. T. (1982). The thickness of the magnetopause current layer: ISEE 1 and 2 observations. *Journal of Geophysical Research*, *87*(A4), 2108–2114. https://doi.org/10.1029/JA087iA04p02108

Cardoso, F. R., Gonzalez, W. D., Sibeck, D. G., Kuznetsova, M., & Koga, D. (2013). Magnetopause reconnection and interlinked flux tubes. *Annales Geophysicae*, *31*, 1853–1866. https://doi.org/10.5194/angeo-31-1853-2013

Cowley, S., & Owen, C. (1989). A simple illustrative model of open flux tube motion over the dayside magnetopause. *Planetary and Space Science*, *37*(11), 1461–1475. https://doi.org/10.1016/0032-0633(89)90116-5

Cowley, S. W. H. (1982). The causes of convection in the Earth's magnetosphere—A review of developments during the IMS. *Reviews of Geophysics and Space Physics*, *20*, 531–565. https://doi.org/10.1029/RG020i003p00531

Ding, D. Q., Lee, L. C., & Ma, Z. W. (1991). Different FTE signatures generated by the bursty single X line reconnection and the multiple X line reconnection at the dayside magnetopause. *Journal of Geophysical Research*, *96*(A1), 57–66. https://doi.org/10.1029/90JA01989

Dorelli, J. C., & Bhattacharjee, A. (2009). On the generation and topology of flux transfer events. *Journal of Geophysical Research*, *114*, A06213. https://doi.org/10.1029/2008JA013410

Dungey, J. W. (1961). Interplanetary field and the auroral zones. *Physics Reviews Letters*, *6*(2), 47–48.

Fear, R. C., Milan, S. E., Fazakerley, A. N., Owen, C. J., Asikainen, T., Taylor, M. G. G. T., . . . Daly, P. W. (2007). Motion of flux transfer events: A test of the cooling model. *Annales Geophysicae*, *25*(7), 1669–1690. https://doi.org/10.5194/angeo-25-1669-2007

Gonzalez, W. D., & Mozer, F. S. (1974). A quantitative model for the potential resulting from reconnection with an arbitrary interplanetary magnetic field. *Journal of Geophysical Research*, *79*(28), 4186–4194.

Haerendel, G., Paschmann, G., Sckopke, N., & Rosenbauer, H. (1978). The frontside boundary layer of the magnetosphere and the problem of reconnection. *Journal of Geophysical Research*, *83*, 3195–3216. https://doi.org/10.1029/JA083iA07p03195

Lee, L. C., & Fu, Z. F. (1985). A theory of magnetic flux transfer at the Earth's magnetopause. *Journal of Geophysical Research*, *12*, 105–108. https://doi.org/10.1029/GL012i002p00105

Lopez, R. E., Bruntz, R., Mitchell, E. J., Wiltberger, M., Lyon, J. G., & Merkin, V. G. (2010). Role of magnetosheath force balance in regulating the dayside reconnection potential. *Journal of Geophysical Research*, *115*, A12216. https://doi.org/10.1029/2009JA014597

Paschmann, G., Haerendel, G., Papamastorakis, I., Sckopke, N., Bame, S. J., Gosling, J. T., & Russell, C. T. (1982). Plasma and magnetic field characteristics of magnetic flux transfer events. *Journal of Geophysical Research*, *87*(A4), 2159–2168. https://doi.org/10.1029/JA087iA04p02159

Powell, K. G., Roe, P. L., Linde, T. J., Gombosi, T. I., & De Zeeuw, D. L. (1999). A solution-adaptive upwind scheme for ideal magnetohydrodynamics. *Journal of Computational Physics*, *154*, 284–309. https://doi.org/10.1006/jcph.1999.6299

Raeder, J. (2006). Flux transfer events: 1. Generation mechanism for strong southward IMF. *Annales Geophysicae*, *24*, 381–392. https://doi.org/10.5194/angeo-24-381-2006

Rijnbeek, R. P., Cowley, S. W. H., Southwood, D. J., & Russell, C. T. (1982). Observations of reverse polarity flux transfer events at the Earth's dayside magnetopause. *Nature*, *300*, 23–26. https://doi.org/10.1038/300023a0

Russell, C. T., & Elphic, R. C. (1978). Initial ISEE magnetometer results—Magnetopause observations. *Space Science Reviews*, *22*, 681–715. https://doi.org/10.1007/BF00212619

Shue, J.-H., Chao, J. K., Fu, H. C., Russell, C. T., Song, P., Khurana, K. K., & Singer, H. J. (1997). A new functional form to study the solar wind control of the magnetopause size and shape. *Journal of Geophysical Research*, *102*, 9497–9512. https://doi.org/10.1029/97JA00196

Sonnerup, B. (1988). Experimental tests of FTE theories. *Advances in Space Research*, *8*(9), 263–272. https://doi.org/10.1016/0273-1177(88)90140-8

Sonnerup, B. U. Ö. (1974). *The reconnecting magnetosphere* (pp. 23–33). Dordrecht, Netherlands: Springer. https://doi.org/10.1007/978-94-010-2214-92

Sonnerup, B. U. Ö., Hasegawa, H., & Paschmann, G. (2004). Anatomy of a flux transfer event seen by Cluster. *Geophysical Research Letters*, *31*, L11803. https://doi.org/10.1029/2004GL020134

Tóth, G., van der Holst, B., Sokolov, I. V., De Zeeuw, D. L., Gombosi, T. I., Fang, F., . . . Opher, M. (2012). Adaptive numerical algorithms in space weather modeling. *Journal of Computational Physics*, *231*, 870–903. https://doi.org/10.1016/j.jcp.2011.02.006

Trenchi, L., Marcucci, M. F., Pallocchia, G., Consolini, G., Bavassano Cattaneo, M. B., Di Lellis, A. M., . . . Cao, J. B. (2008). Occurrence of reconnection jets at the dayside magnetopause: Double star observations. *Journal of Geophysical Research*, *113*, A07S10. https://doi.org/10.1029/2007JA012774

Trenchi, L., Marcucci, M. F., & Fear, R. C. (2015). The effect of diamagnetic drift on motion of the dayside magnetopause reconnection line. *Geophysical Research Letters*, *42*(15), 6129–6136. https://doi.org/10.1002/2015GL065213